Biomechanical Analysis of the Slow-Twitch (Red) Muscle Force Transmission Pathways in Tunas*

Melinda J. Cromie Lear[1,†]
Matthew Millard[1,†]
Adrian C. Gleiss[2,3]
Jonathan Dale[2]
Marina Dimitrov[1,2]
Elizabeth Peiros[1,2]
Barbara Block[2,‡]
[1]Mechanical Engineering, Stanford University, California; [2]Hopkins Marine Station, Stanford University, California; [3]Centre for Sustainable Aquatic Ecosystems, Harry Butler Institute, Murdoch University, 90 South Street, Murdoch, Western Australia, Australia, and College of Science, Health Engineering and Education, Murdoch University, 90 South Street, Murdoch, Western Australia, Australia

Accepted 1/11/2020; Electronically Published 3/20/2020

Online enhancements: supplemental tables.

ABSTRACT

In tunas, the slow-twitch red muscle, which has an elevated temperature, powers thunniform locomotion, a stiff-bodied swimming style. The anatomical placement and operating temperatures of red muscle vary widely among teleosts: in tunas, the red muscle is located centrally in the body, adjacent to the spine, and maintains an elevated temperature. In the majority of ectothermic teleosts, red muscle is located laterally in the body, adjacent to the skin, and operates at ambient temperature. The specialized physiology and biomechanics of red muscle in tunas are often considered important adaptations to their high-performance pelagic lifestyle; however, the mechanics of how muscular work is transmitted to the tail remains largely unknown. The red muscle has a highly pennate architecture and is connected to the spine through a network of bones (epicentral bones) and long tendons (posterior oblique tendons). The network of long tendons has been hypothesized to enhance the power transmitted to the tail. Here, we investigate the morphology and biomechanics of the tuna's red muscle and tendons to determine whether elasticity is exploited to reduce the cost of transport, as is the case in many terrestrial vertebrates. To address this question, we evaluate two hypotheses: (1) tendons stretch during red-muscle-actuated swimming and (2) tendons comprise the primary load transmission pathway from the red muscle to the spine. To evaluate these hypotheses, we measured the mechanical properties of the posterior oblique tendons and performed novel dissections to estimate the peak force that the red muscle can generate. The force-generating capacity of the red muscle is calculated to be much greater than the load-bearing capacity of the posterior oblique tendons. Thus, the long tendons likely stretch under force from the red muscle, but they are not strong enough to be the primary force transmission pathway. These results suggest that other pathways, such as serial load transmission through the red muscle myomeres to the great lateral tendon and/or the anterior oblique tendons to the skin, transmit appreciable force to the tail.

Keywords: musculoskeletal anatomy, thunniform locomotion, tendon mechanical properties.

*This paper was submitted in response to a call for papers for a Focused Issue on "Functional Morphology and Biomechanics: Form Follows Function."

†These authors contributed equally.

‡Corresponding author; email: bblock@stanford.edu.

Physiological and Biochemical Zoology 93(3):185–198. 2020. 1522-2152/2020/9303-9043$15.00. DOI: 10.1086/708247

Introduction

Tunas are renowned for extensive transoceanic migrations, traveling thousands of kilometers as they move between foraging and spawning grounds and swimming continuously at rates of one to three body lengths per second (Korsmeyer and Dewar 2001; Gleiss et al 2019). All tunas swim with a stiff body motion referred to as "thunniform locomotion," characterized by minimal lateral movement or bending of the anterior portion of the body with thrust largely generated by the tail (Altringham and Shadwick 2001). Thunniform swimming exists on one end of a continuum of swimming movements ranging from eel-like locomotion, where multiple wavelengths of bending are present along the body, to thunniform locomotion, where less than one wavelength of bending is present along the body (Altringham and Shadwick 2001). Externally, tuna have a streamlined body shape and a lunate tail (fig. 1*A*). The streamlined shape minimizes drag forces (Triantafyllou et al. 2005; Cipolla 2014). The lunate tail is well suited for efficient thrust generation with a high lift-to-drag ratio (Altringham and Shadwick 2001). Internally, thunniform swimming is powered by red muscle with three features that differ from most other teleosts: (1) elevated red muscle temperature, (2) medially located red muscle, and (3) a network of bones and tendons connecting the red muscle to the spine.

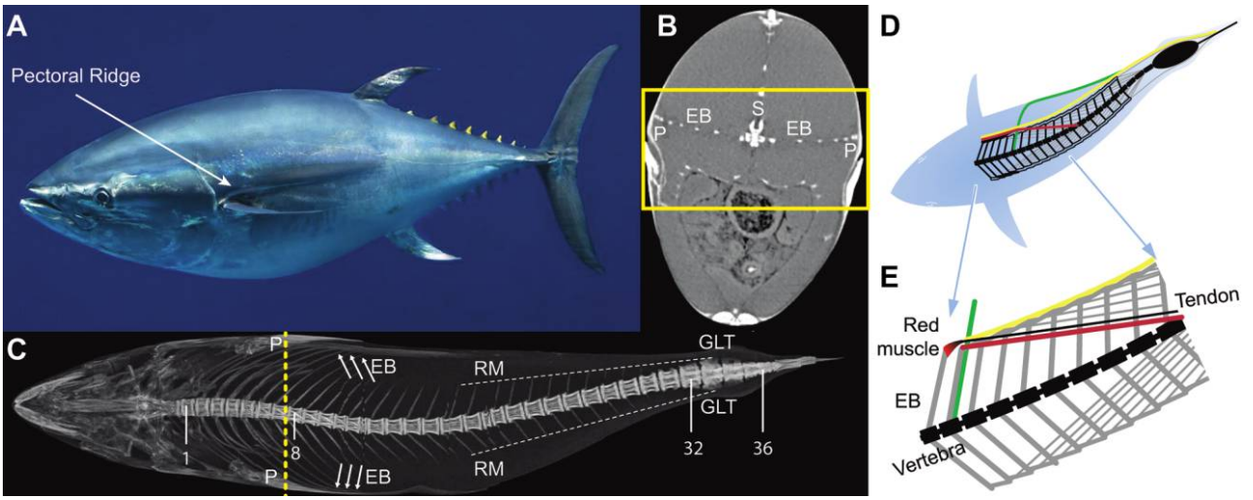

Figure 1. Tuna skeletal structure reveals key features of thunniform swimming. *A*, Exterior view of pectoral ridge, where anterior epicentral bones anchor to the lateral body wall. Photograph by Randy Wilder, Monterey Bay Aquarium. *B*, Cross-sectional computed tomography (CT) scan showing the epicentral bones (EB) in the horizontal plane with the spine (S) and pectoral ridge (P). Epicentral bones are visible in cross section as high-contrast dots along the horizontal plane. Boxed area shows the portion of the images used to create the projection in *C*, focusing on the spine and epicentral bones within the horizontal septa. *C*, Dorsoventral projection of the CT scan of a Pacific bluefin tuna. Epicentral bones attach medially to the spine at the anterior end of the associated vertebra. Three epicentral bones (EB) on each side are indicated with arrows. White dashed lines trace the center of the red muscle (RM) to the wrapping point of the great lateral tendon (GLT) at the broadest point of the posterior vertebrae. Note that the broadest point of the posterior vertebrae is anterior to the broadest point of the exterior fleshy peduncle. Compare with dissection photograph in figure 2*E*. Points of discontinuity in the images are due to missing image slices in the CT scan. Image slice from *B* indicated by yellow dashed line. Numbers indicate vertebrae number. *D*, *E*, Diagram of load transmission pathways showing whole-body view (*D*) and enlarged view (*E*). One load transmission pathway (red) is from the red muscle myomere to the spine via the posterior oblique tendons. A second load transmission pathway (yellow) is serially through the red muscle myomeres and into the GLT and tail. A third load transmission pathway (green) may involve the anterior oblique tendons alongside the epicentral bones (EB) to the skin and tail.

The red muscle temperature is elevated above the temperature of the surrounding tissue and surrounding environment, a condition called "regional endothermy" (Carey and Teal 1966; Carey and Lawson 1973; Graham and Dickson 2001). Regional endothermy is also found in lamnid sharks (Carey et al. 1985), but most other teleosts are ectothermic. In tunas, a countercurrent heat exchanger separates the red and white muscle layers and conserves the metabolic heat from red muscle contractile activity (Kishinouye 1923; Carey and Teal 1966). The elevated red muscle temperature could double the muscle power output, as predicted by physiological studies (yellowfin tuna; Altringham and Block 1997). Selective pressure favoring expansion of the thermal niche (latitude and depth) within which tunas can forage and hunt may have had a role in selection for anatomical specializations that led to regional endothermy (Block et al. 1993; Graham and Dickson 2000, 2001; Dickson and Graham 2004).

The red muscle in the tuna is medially located, as opposed to laterally located under the skin as in other teleosts (Westneat and Wainwright 2001; Katz 2002). The muscles of many fish species are arranged in layered cones (Videler 1993; Shadwick and Gemballa 2006). In tuna, the cone morphology is specialized to be elongated (Westneat and Wainwright 2001), enabling high cross-sectional area and therefore high force-generating capacity in the muscle (Katz 2002). The medial red muscle is also part of this cone structure. The structure of tuna red muscle may have arisen by white muscle within the cone structure beginning to express the red muscle phenotype (Katz 2002). This morphology may thereby have given the advantage of packing more red muscle volume into the fusiform body anatomy (Katz 2002). A key metric for evaluating muscle contribution to locomotion is the force-generating capacity related to the physiological cross-sectional area and the tensile stress that the muscle can generate (e.g., Lieber 2010). However, the physiological cross-sectional area of tuna red muscle within this unique morphology has not been examined.

The third noteworthy musculoskeletal feature is the network of long tendons (posterior oblique tendons [POT]) and bones (epicentral bones) that connect the red muscle to the spine and tail (Westneat and Wainwright 2001; figs. 2*C*, 3*D*, 3*E*). This network is a specialization of the horizontal septum. The horizontal septum, a layer of connective tissue, is common in many fish, with morphologies ranging from sheets of collagen to distinct tendons to ossified tendons (Gemballa et al. 2003). The bones within the horizontal septa have been called "epicentral bones" (Gemballa et al. 2003), "intramembranous ossification of the anterior oblique tendons" (Gemballa et al. 2003), and "epipleural bones" (Westneat et al. 1993). Throughout the article, we will use "epicentral bones." The POTs are connected to the collagen-rich sheets called "myosepta" that separate the muscle cones (Westneat and Wainwright 2001). The myosepta transfer muscle load serially between myomeres. Each POT

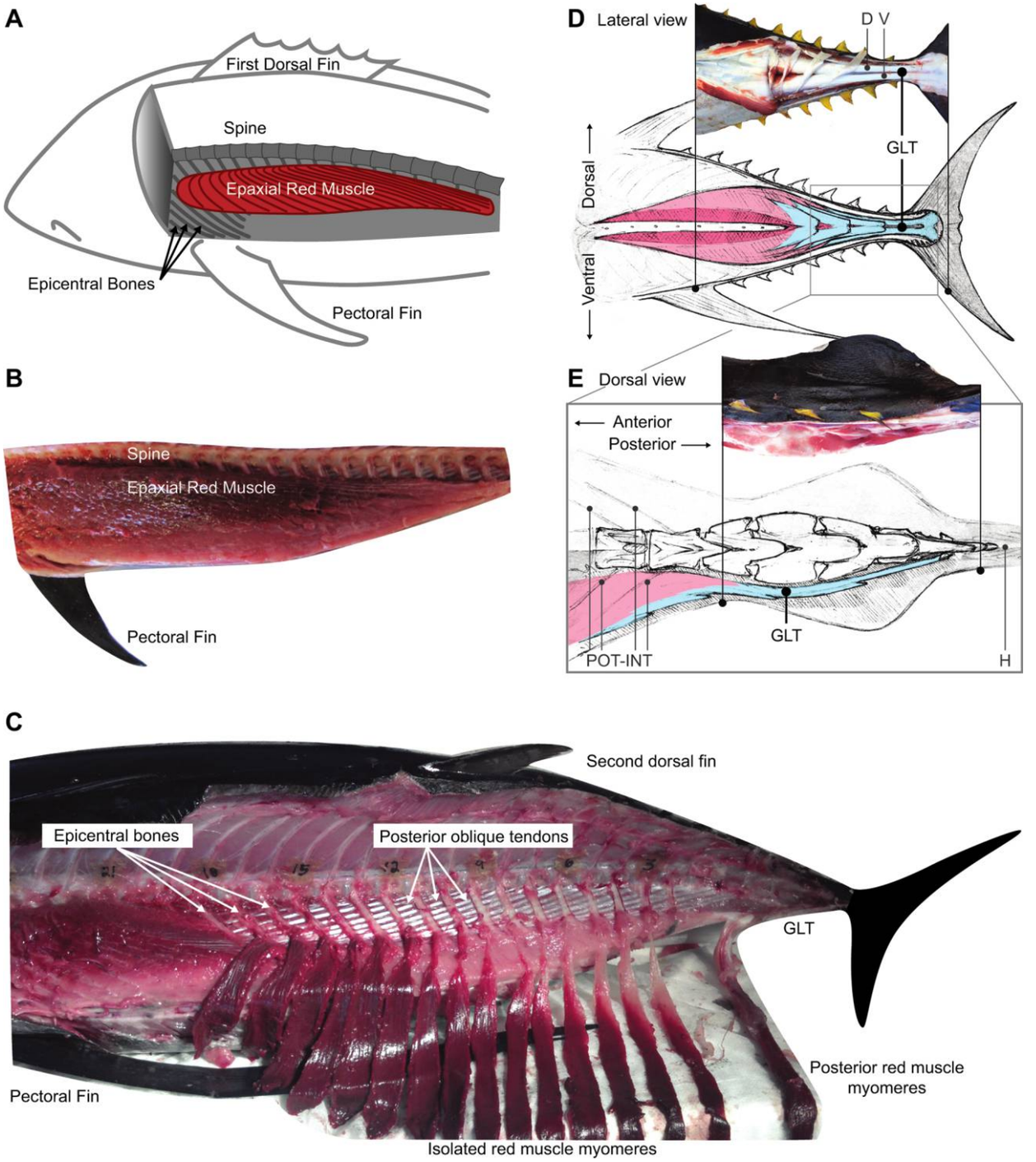

Figure 2. Dissection and measurements to visualize load transmission morphology and measure red muscle cross-sectional area. *A*, *B*, Diagram (*A*) and photograph (*B*) of dissection stage 1. This dissection enables view of intact epaxial red muscle to examine form and function relative to thunniform swimming motion. The red muscle is composed of individual myomeres layered on one another (Pacific bluefin). *C*, Dissection stage 2. Dissection of red muscle separated into individual myomeres to examine repeating myomere-bone-tendon units (albacore). Note that intermediate red muscle myomeres are each attached to an epicentral bone and a posterior oblique tendon (POT). The most posterior red muscle myomeres do not attach to epicentral bones or POTs and instead attach to the great lateral tendon (GLT), which inserts on the caudal fin. *D*, Lateral view, dissection photograph (inset) and diagram of the GLT in a yellowfin tuna. The GLT (light blue) has a dorsal (D) and ventral (V) collagen bundle. The GLT has connection with white muscle (lighter red), red muscle (medium red), and collagen of the skin. *E*, Dorsal view, dissection photograph (inset) and diagram of the GLT in a yellowfin tuna. The GLT connects to the posterior myomeres (two representative posterior myomeres [M]; cf. *C*), wraps around the lateral edge of the broadened vertebrae, and inserts on the tail at the hypural plate (H). In the inset dissection photograph, the right side of the fish (*top*) shows the exterior fleshy keel, and the left side of the fish (*bottom*) has been dissected to show the broad posterior vertebrae around which the GLT wraps. Compare with posterior vertebrae shown in the CT projection in figure 1*C*.

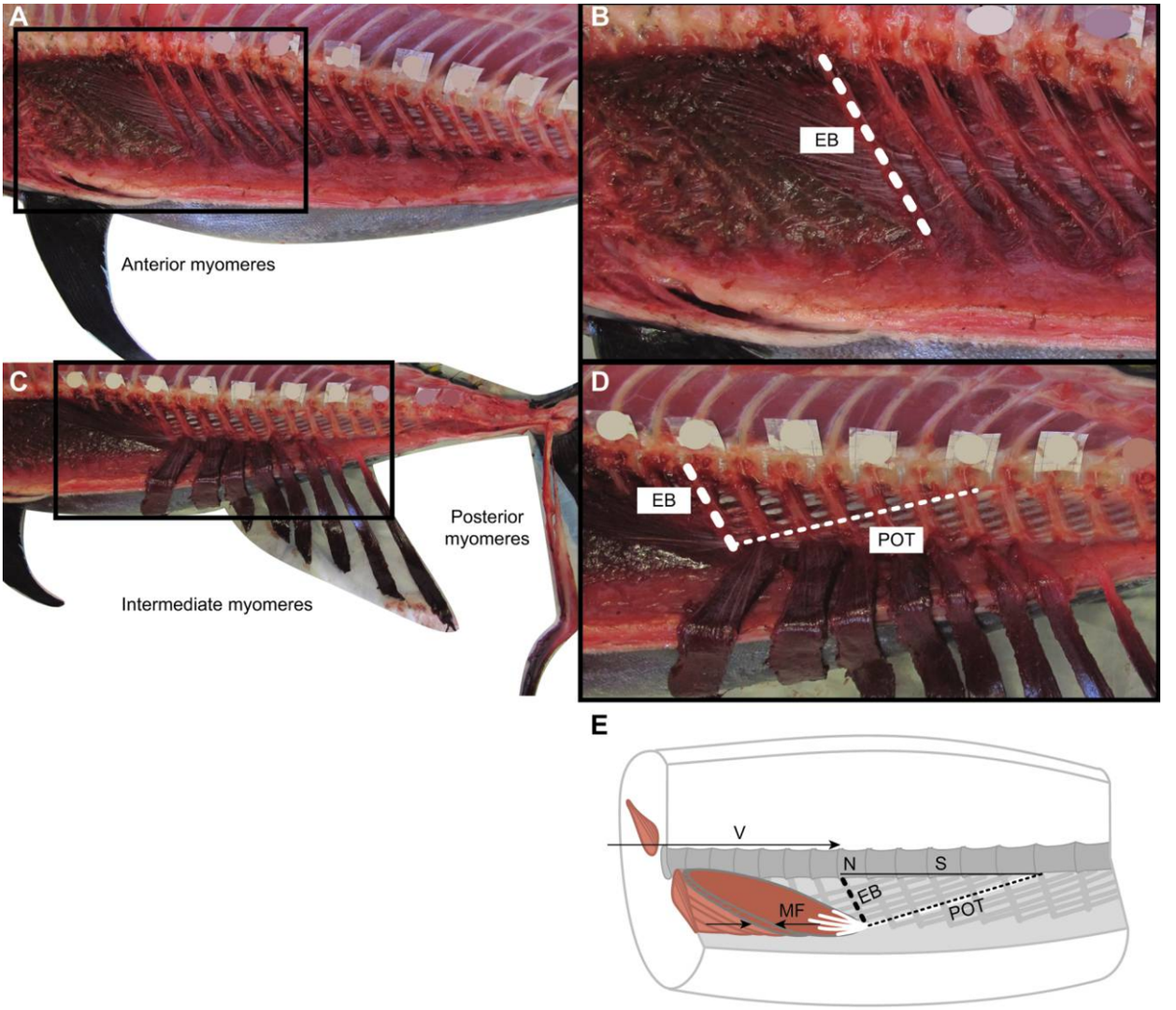

Figure 3. Red muscle myomeres transmit load via myosepta to adjacent myomeres and tendons. *A*, Anterior myomeres. *B*, Enlarged view of boxed area in *A*. The distance along the epicentral bone (EB) to the estimated centroid of the collagen was the measurement used in figure 4. *C*, Intermediate and posterior myomeres. Note that the posterior myomeres do not have associated epicentral bones or posterior oblique tendons but instead directly merge with the great lateral tendon, which actuates the lateral movement of the tail. *D*, Enlarged view of boxed area in *C*, showing epicentral bone (EB) and posterior oblique tendon (POT). *E*, Anatomical measurements. Measurement of the length of the epicentral bone (EB), posterior oblique tendon (POT), and muscle fiber (MF) of each myomere-bone-tendon (MBT) unit. Note that the muscle fiber direction is through the thickness of the myomere, aligned with the anterior-posterior axis of the fish. Measurement of the distance along the spine (S) between the bone attachment and the insertion of the tendon of the same MBT unit, the vertebra number (N), and the position of the vertebra (V) along the anterior-posterior axis from a fixed reference on the spine at the anterior position of the pectoral fin.

attaches to the spine posterior to the associated red muscle. The most posterior red muscle myomeres do not have POTs and are instead connected to the tail via the great lateral tendons (GLT; figs. 2*C*, 3*C*). Westneat et al. (1993) also reports a third potential load transmission pathway in scombrids called the "anterior oblique tendons" (AOTs). The AOTs are closely integrated with the epicentral bones, myosepta, and skin (Westneat et al. 1993; Westneat and Wainwright 2001).

The function of POTs in locomotion cannot be inferred from morphological studies alone, in part because POTs are found in combination with a variety of anatomical and physiological traits across species with different locomotory styles. In tunas, the POTs have been hypothesized to enable the uncoupling of the red muscle strain from the body-bending strain (Knower et al. 1993; Katz et al. 2001; Shadwick and Syme 2008) and to tune the biomechanical advantage of the medially located red muscle (Westneat et al. 1993; Westneat and Wainwright 2001). Several species of mackerel, bonito, and wahoo have distinct POTs (Fierstine and Walters 1968; Westneat et al. 1993). In contrast to the medial red muscle of tunas, mackerels have laterally located red muscle (Fierstine and Walters 1968; *Scomber scombrus* [Westneat et al. 1993]), and bonitos have an intermediate

distribution with some medial red muscle (*Sarda chiliensis*; Ellerby et al. 2000). Also in contrast to tunas, mackerels and bonitos swim with carangiform locomotion (e.g., *Scomberomorus cavalla*, *Scomberomorus maculatus*, *Scomber scombrus*, and *Sarda Sarda* [Westneat et al. 1993]; *Sarda chiliensis* [Ellerby et al. 2000]) and are not endothermic (Ellerby et al. 2000; Westneat and Wainwright 2001; Dickson and Graham 2004). Westneat and coauthors (1993) summarize the phylogenetic trends in the POTs across seven species studied, with the observation that the POTs of mackerels tend to be band-like, have larger angles to the spine, and cross fewer vertebrae, whereas the POTs of tunas are cord-like, have smaller angles to the spine, and cross more vertebrae. The POTs of bonitos, an intermediate species between tunas and mackerels, have an intermediate shape and intermediate angles. Westneat et al. (1993) and Ellerby et al. (2000) modeled how the tendon lengths and angles could affect the transfer of muscle force and speed to the bending of the spine. However, the models assume that the tendons bear a substantial component of the red muscle load to the spine. Outside the scombrid family, strain in the medial red muscle in two species of sharks is also decoupled from body bending, and long tendon-like collagen structures within the myosepta are observed connecting the red muscle to the posterior spine (shortfin mako, *Isurus oxyrinchus* [Donley et al. 2004, 2005]; common thresher shark, *Alopias vulpinus* [Bernal et al. 2001, 2010]). However, in other lamnid sharks, red muscle is also medially located and regionally endothermic (e.g., Carey et al. 1985), but it does not appear to have associated tendon-like structures (Donley et al. 2004). Distinct tendons are also found in the horizontal septa of the zebra fish, *Danio rerio* (Gemballa et al. 2003), a small, ectothermic, freshwater fish commonly used as a laboratory model organism. The in vivo function of the POTs depends on their mechanical properties and loading dynamics during locomotion, which are unknown.

The POTs are long compared with the fiber lengths of the associated red muscle. Thus, the tendons are an important biomechanical feature because of their potential impact on swimming economy. In terrestrial animals, long compliant tendons can stretch to allow muscle fibers to maintain an optimal fiber length over a larger range of joint motion (Arnold et al. 2010; Arnold and Delp 2011). Long tendons can also rapidly recoil, allowing fibers to shorten at lower velocities and thus consume less metabolic energy (Biewener et al. 1998). In tunas, red muscle operates at length ranges and velocities that optimize its work output (Shadwick and Syme 2008; Syme and Shadwick 2011). Although the fiber strain of the red muscle has been measured in vivo in yellowfin tunas during sustained swimming (Shadwick and Syme 2008), the tendon kinematics are unknown.

We hypothesize that the medially located red muscle and the network of tendons and bones provide biomechanical advantages for swimming economy, and we examine the structure and function of the musculoskeletal system in this context, using new measurements of musculoskeletal anatomy and tendon mechanical properties. Since it is challenging to measure the load developed and transmitted by these tissues in vivo, we instead make use of data obtained by dissection, biomechanical analysis, and material testing to determine how much of the red muscle's tension is transmitted through the tendons. We indirectly address this hypothesis by examining whether the properties of the tendon and the red muscle are consistent with those observed in terrestrial animals (Biewener et al. 1998) in which long tendons affect muscle fiber dynamics. First, we examine whether the tendons are capable of stretching large fractions of a fiber length under a physiological load. Second, we examine whether the tendons are strong enough to bear more than the maximum isometric tension that the red muscle should be capable of generating. If the tendons are the primary load pathway for the muscle, it must be the case that the tendons are physically capable of sustaining the peak loads developed by the red muscle.

To address these questions, we developed a dissection to isolate and measure the physiological cross-sectional area of the red muscle portions of the cones to evaluate the red muscle's force-generating capacity. We measured the musculoskeletal geometry of tuna red muscle, POTs, epicentral bones, and spine. We isolated and measured the tensile mechanical properties of the POTs. The AOTs are integrated with the epicentral bone and the myosepta as a distributed collagen mesh and thus were not amenable to dissection and tensile testing. To address our hypotheses about the locomotory function, we compared the force-generating capacity of the muscle with the load-bearing capacity and elongation of the POTs.

Methods

Fish Acquisition and Maintenance

This research was carried out at the Tuna Research and Conservation Center (TRCC), a collaborative facility of Hopkins Marine Station of Stanford University and the Monterey Bay Aquarium. The Pacific bluefin (*Thunnus orientalis*) and albacore tuna (*Thunnus alalunga*) used in this study were acquired and maintained in accordance with protocols for tunas at the TRCC, which were approved by the Stanford University Administrative Panel on Laboratory Animal Care (APLAC). They were collected from the wild in accordance with the California Department of Fish and Game and/or Mexican collection permits in the California current off the western coast of North America, acclimated to a tank at 20°C or 18°C, and euthanized under Stanford APLAC-approved protocols for organ tissue collection for other studies. Fresh specimens were used for myomere dissections and tendon mechanical measurements. Specimen lengths and measures taken on each specimen are given in table S1 (tables S1, S2 are available online).

Computed Tomography (CT) Scan

To capture a view isolating the spine and epicentral bones within the whole fish, a fresh specimen was scanned with transverse image slices at 1-mm slice spacing (fig. 1*B*) on a Siemens Somatom Volume Zoom CT scanner at the Computerized Scanning and Imaging Facility of Woods Hole Oceanographic Institution. A segment of each image slice near the horizontal septum was

used to reconstruct a dorsoventral projection using ImageJ (Schindelin et al. 2012; Rueden et al. 2017; fig. 1*C*).

Dissection

We developed a two-stage dissection to enable measurement of the physiological cross-sectional area (PCSA) of red muscle and to visualize the intact red muscle, bones, and tendons as a complete biomechanical system (fig. 2*A*, 2*B*) and as a series of repeated units (fig. 2*C*). Each myomere-bone-tendon (MBT) unit comprised a red muscle myomere, the associated epicentral bone, and the connecting tendon. The dissection enabled us to measure the musculoskeletal geometry of the MBT units and estimate the peak force that each red muscle myomere can generate.

Dissection Stage 1. In the first stage of the dissection, we visualized the red muscle intact and in connection with the horizontal septa (fig. 2*A*, 2*B*). We first cut along the dorsal ridge through the skin, immediately lateral to the dorsal fins. We blunt dissected the epaxial white skeletal muscle away from the collagenous vertical septa. The fast-twitch white muscle was retracted until the spine was visualized. We next opened a lateral approach by cutting the skin dorsal to the ridge at the pectoral fins. Because the anterior-most bones insert into this ridge, this anatomical landmark ensures an incision dorsal to the anterior-most bones. We removed the skin to visualize the cutaneous arteries and veins. Using the dorsal cutaneous artery as a starting point and following the membrane that separates the red and white muscle, we separated the white muscle from the red muscle using blunt dissection. The membrane contains the vessels of the *rete mirable*, which functions as a countercurrent heat exchanger to elevate red muscle temperature (Graham and Dickson 2001). The larger fish had collagenous filaments crossing the *rete mirable*, which were cut with a scalpel. We opened the border of red and white muscle moving medially toward the spine, thus leaving the red muscle in place on the bones. When the lateral and dorsal approaches met near the spine, the white muscle was removed, leaving the intact red muscle in place in the fish. This exposure allowed us to examine the epaxial red muscle as a whole, its interconnection to the skeleton and connective tissue, and its form and function in thunniform locomotion.

Dissection Stage 2. We then blunt dissected one myomere at a time from the underlying myomere (figs. 2*C*, 3). We worked posterior to anterior because each myomere lies dorsally on its anterior neighbor. We later isolated and measured the area, length, and width of each myomere. This exposure allowed us to examine the anatomy and measure the geometry of each MBT unit and to observe in detail the force-generating and force-transmitting structures.

Musculoskeletal Geometry

In the second stage of the dissection, working posterior to anterior, we measured the geometric properties of each MBT unit on one side of each fish (fig. 3*E*). We collected these measurements in seven tunas: five *T. orientalis* (Pacific bluefin) and two *T. alalunga* (albacore). Not all measurements were taken on all specimens; see table S1.

Using calipers, we measured the length of the bone, tendon, and muscle fiber of each MBT unit (fig. 3*E*). We recorded the distance along the spine between the bone attachment and the insertion of the tendon of the same MBT unit (fig. 3*E*). We also measured the position of each vertebra along the anterior-posterior axis from a fixed reference on the spine at the anterior position of the pectoral fin (fig. 3*E*). We measured the attachment points of the tendons on the bones (figs. 3*E*, 4*A*). Musculoskeletal geometry measurements are included in table S2.

To measure the myomere PCSA, we positioned each isolated myomere on graph paper with quarter-inch markings and photographed it. Myomere PCSA and aspect ratio (length divided by width) were measured from the images, using the grid as a calibration for each image (fig. 5*A*, 5*B*). The myomere area is a good approximation of the PCSA because the short muscle fibers run through the thickness of the myomere. Measurements were made on dissected fresh specimens. We measured only the epaxial (dorsal) red muscle myomeres. Tunas also have hypaxial (ventral) red muscle myomeres that converge on the same POTs (Fierstine and Walters 1968; Westneat et al. 1993; Korsmeyer and Dewar 2001). The hypaxial red muscle appears to have a volume and distribution similar to the epaxial red muscle in our own dissections and in published cross-sectional diagrams (e.g., Fierstine and Walters 1968; Westneat et al. 1993), but this has not been directly measured to our knowledge.

We calculated the ratio of tendon length to red muscle fiber length (tendon length divided by myomere fiber length) from the measured values. This ratio is related to whether the tendon stretch will be significant when compared with the fiber length of the muscle (Biewener and Roberts 2000).

Tendon Mechanical Properties

We measured the mechanical properties of 20 POTs from a Pacific bluefin tuna. Tendons were collected immediately after euthanasia, frozen at –20°C, shipped on dry ice, and kept frozen at –20°C until testing. The tendons were gripped in cryogrips cooled with liquid nitrogen using methods similar to those described by Sharkey et al. (1995). Tensile tests were performed on a TA Instruments Electroforce 3230 equipped with a physiological water bath at 25°C and using WinTest 7 software (Zymetrix, Calgary, Alberta). Note that freeze-thaw cycles do not significantly affect the tensile properties of ligaments and tendons (Moon et al. 2006; Huang et al. 2011; Jung et al. 2011). The temperature of the POTs in vivo can be assumed to follow that of the surrounding red muscle, which could be from 4° to 20°C above ambient water temperature (Carey and Lawson 1973; Dewar and Graham 1994). Previous tests of tuna GLT were conducted in air without specifically controlling temperature (Shadwick et al. 2002). Human shoulder tendons (supraspinatus) tested across a range of 17° to 42°C did

not show differences in elastic parameters across this range (Huang et al. 2009). We tested the tendons to failure and measured the force and displacement over time. The steady state displacement was controlled to 0.333 mm/s with a ramp-up period of 1 s. With slightly different grip-to-grip distances across specimens, the median steady state strain rate was 0.87 %/s (minimum: 0.61; maximum: 2.18). In previous investigations of mammalian tendons, Young's modulus was not affected by strain rate (Bennett et al. 1986). To calculate stress and strain from the force-displacement curve, we normalized by the cross-sectional area and the tested length (grip-to-grip distance). Tendon cross-sectional area was approximated by a rectangle with the same thickness and width. From the stress-strain curves, we calculated the maximum tangent stiffness, which we assumed to be the onset of plastic deformation. We calculated the tangent stiffness, strain, stress, and total energy absorbed at the onset of plastic deformation. Tensile failure was defined as the point at which the slope of the stress-strain curve passed through zero from positive to negative. We calculated the strain, stress, and total energy absorbed (toughness) at failure.

Results

Synthesis of the CT scan projection (fig. 1*C*) and measurements of the location of tendon attachments to the bone (fig. 4*B*) showed two previously undocumented anatomical features. First, the epicentral bones systematically decrease in length from head to tail. Second, the anterior epicentral bones anchor to the lateral edge of the fish at the pectoral fins (see the dashed yellow line near the pectoral fin in fig. 1*C*).

The musculoskeletal dissections and measurements revealed previously undocumented changes in the aspect ratio of the red muscle myomeres along the length of the fish and between fish (fig. 5). Example myomere cross sections demonstrate the trend that posterior myomeres, within the narrow tail of the fusiform fish, are elongated, while anterior myomeres, in the broadest area of the fish, are wider and shorter (fig. 5*C*, 5*E*). A surprising finding was that in the smallest fish (79 cm), the myomere area was constant from anterior to posterior, whereas the larger fish (123 and 166 cm) had greater physiological cross-sectional areas posteriorly (fig. 5*D*). The aspect ratio changed with

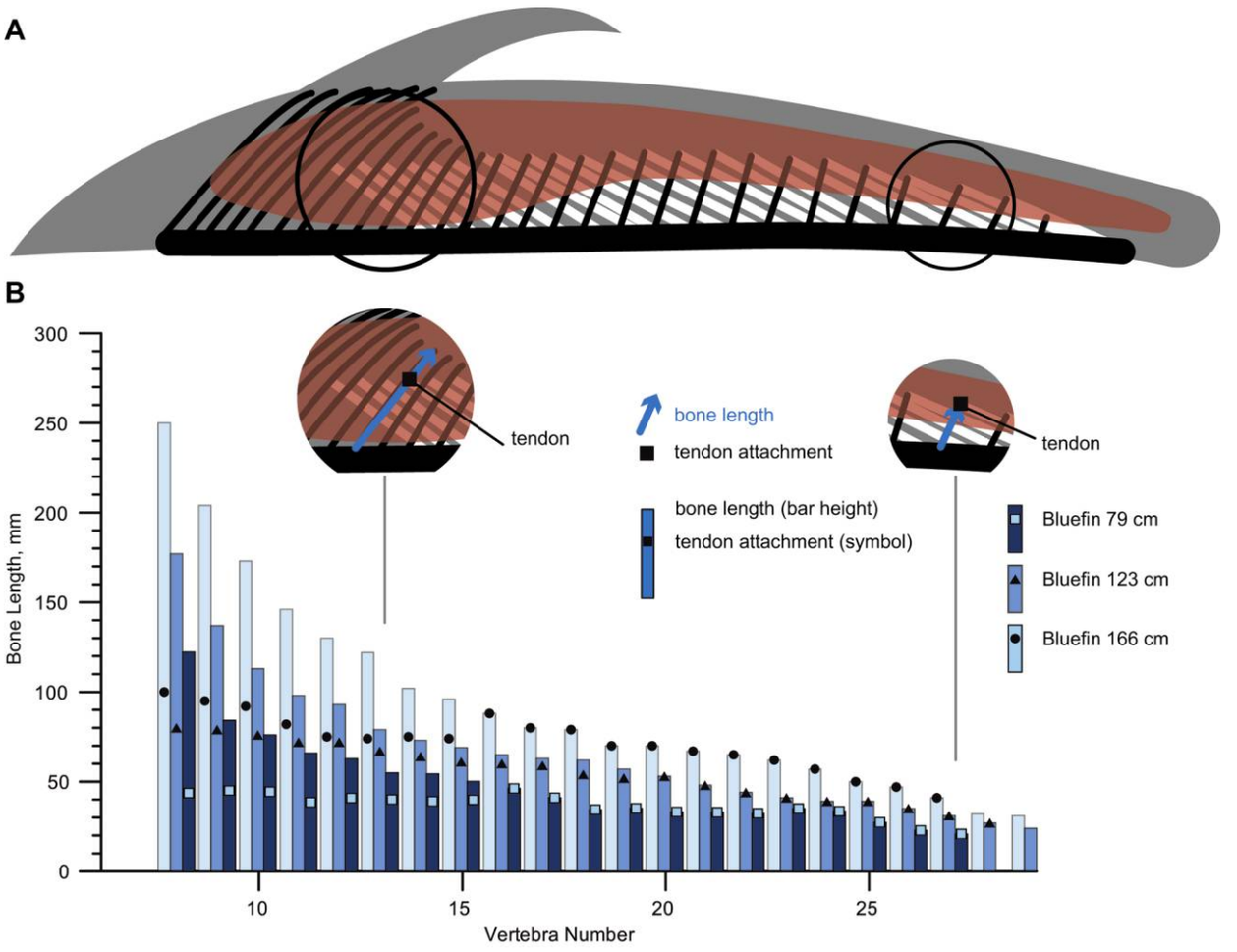

Figure 4. Epicentral bones and tendon attachment points change systematically with anterior-posterior location. *A*, Diagram of measurements. Red indicates total red muscle mass, black indicates spine and epicentral bones, and white indicates tendons. Circles indicate highlighted areas in *B*. *B*, Epicentral bone lengths and tendon attachment points vary along the length of the body.

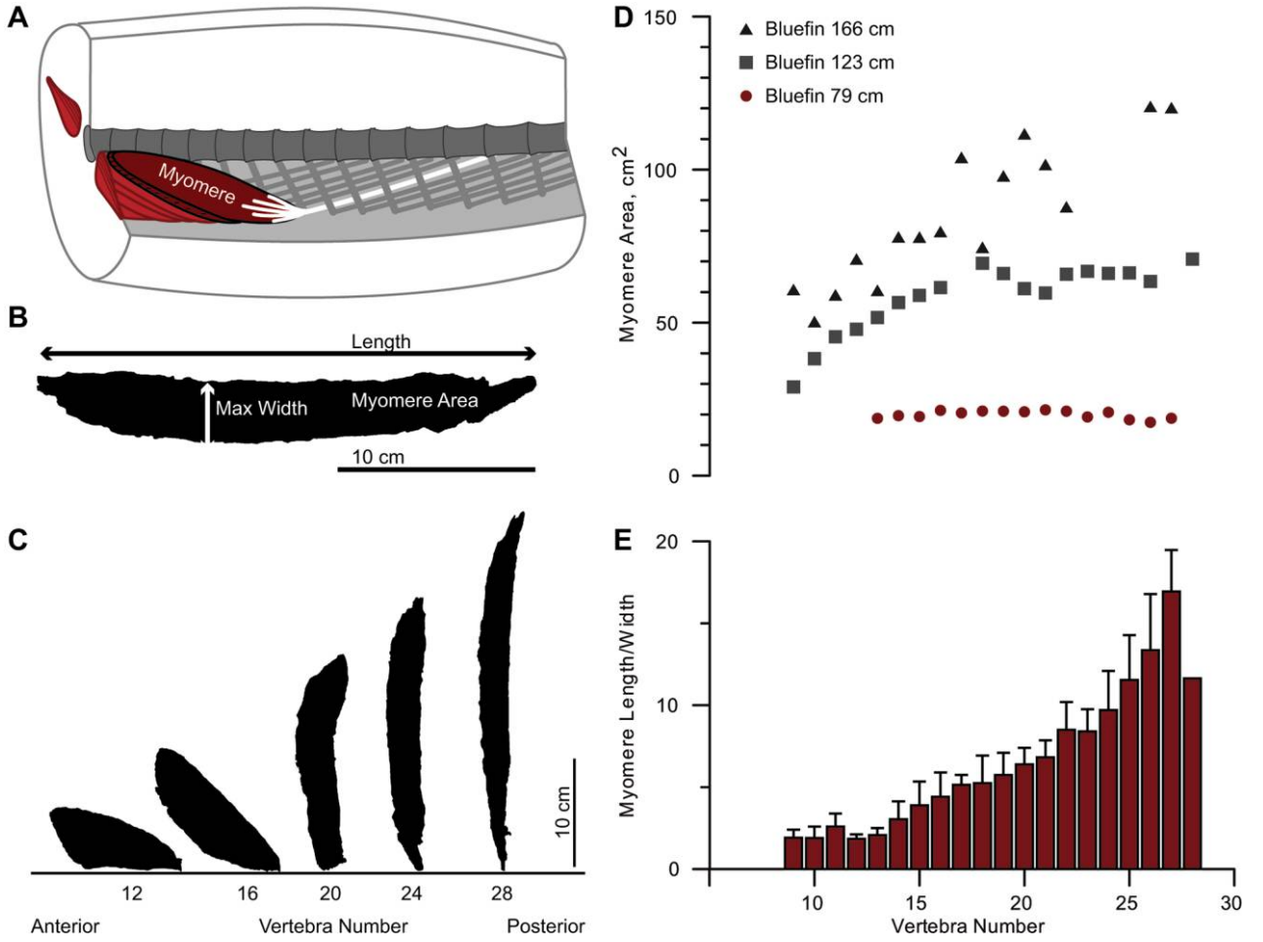

Figure 5. Morphology and physiological cross-sectional area of red muscle myomeres. Red muscle myomeres are located medially and have an elongated shape. *A*, Diagram of myomere location within a myomere-bone-tendon (MBT) unit within the fish. Epicentral bones are shown in dark gray. Posterior oblique tendons are shown in light gray. The posterior oblique tendon associated with the highlighted MBT unit is shown in white. *B*, Myomere area, length, and width were measured from photographs of isolated myomeres, using graph paper for scale. *C*, Representative myomere outlines from the 79-cm Pacific bluefin illustrate the trend of an increasing aspect ratio and similar area from anterior to posterior. *D*, Myomere areas from three bluefins of different lengths (79, 123, and 166 cm). The 79-cm bluefin has nearly identical myomere areas anterior to posterior. In the larger fish, the posterior myomeres are twice the area of the anterior myomeres. *E*, Independent of fish size, the aspect ratio of the myomeres increases similarly anterior to posterior ($n = 3$ specimens, the same specimens as in *D*).

anterior-posterior position but did not vary between fish of different sizes (fig. 5*E*). Finally, we confirmed that for these species, the most posterior red muscle segments of myomeres are also connected from their anterior myomere neighbors directly to the GLT with no epicentral bones or POTs (fig. 2*C*).

Measurements of the MBT functional units revealed that the tendon lengths vary from anterior to posterior. The tendons were longest in the midbody of the fish and were up to 20-fold longer than the muscle fibers (fig. 6). The tensile testing of the tendons revealed that at the point of maximum tangent stiffness, the tendons experienced an elongation of 2.9% ± 1.4% under a load of 21.3 ± 10.8 N (fig. 7; table 1). Assuming a peak stress-generating capacity of 14.0 N/cm^2 (Syme and Shadwick 2002), the myomeres can generate maximum isometric tensions of 273 ± 32 N given the areas of 19.5 ± 2.3 cm^2 that we measured in a similar-sized fish (fig. 5*D*). The measurements indicate that the myomeres would need to be activated by only approximately 7% (generate 7% of their maximum isometric tension) in order to generate forces that would stretch the tendons to the inflection point. Using tendon lengths and muscle fiber lengths from the 79-cm bluefin, an average tendon strain of 2.9% would result in a tendon length change of 3.1 ± 0.4 mm, which is more than 38% ± 7% of the muscle fiber length. This percentage of tendon extension to fiber length is much higher than the 20% threshold identified by Biewener and Roberts (2000) as favoring elastic energy storage over control.

The failure load of the tendons is far lower than the maximum isometric force the myomeres can generate, refuting our second hypothesis that the tendons bear most of the load from the myomeres. The tendons failed at 33 ± 21 N, which is substantially lower than the estimated maximum isometric force of 273 ± 32 N that the myomeres can generate. Although the tendons cannot bear the full tension of the myomeres, the tendons are quite tough: the failure toughness of an

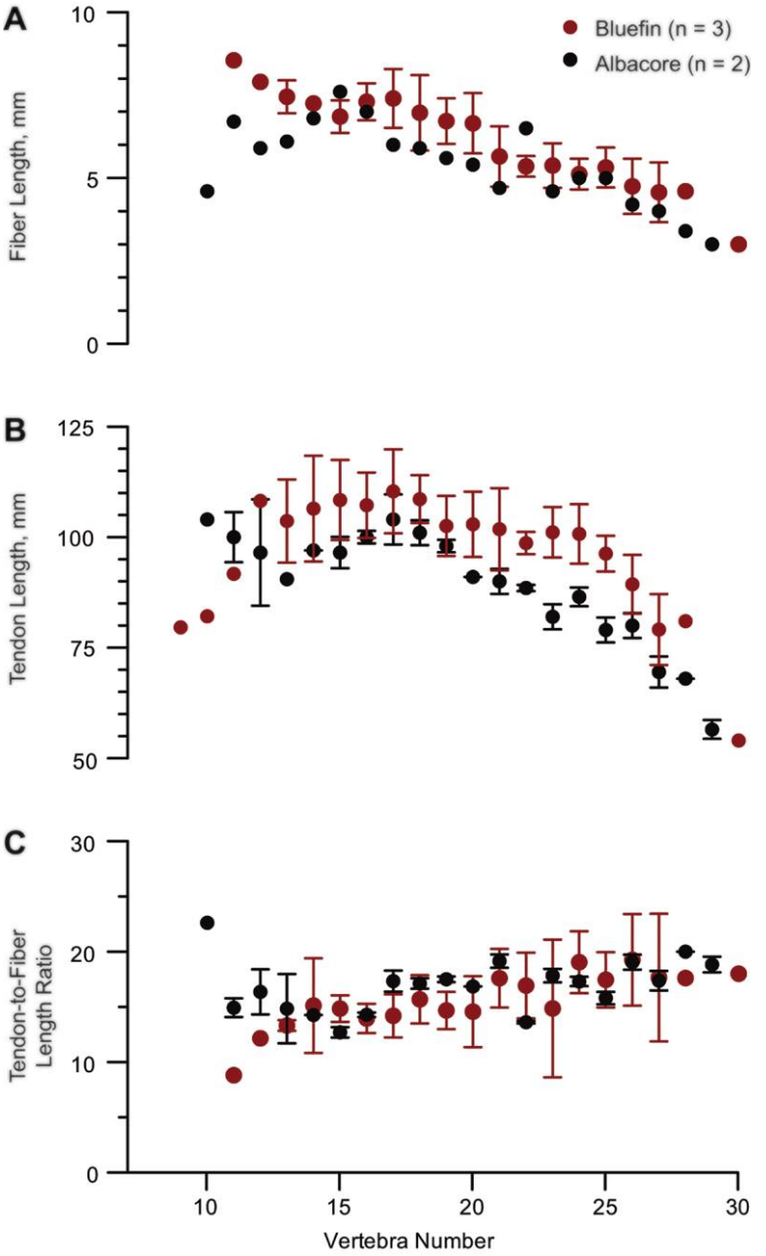

Figure 6. Lengths of red muscle fibers and posterior oblique tendons. *A*, Myomere fiber lengths decrease posteriorly in both species (bluefin: 60, 79, and 82 cm; both albacore: 68 cm). *B*, Tendons are longest in the intermediate range where most of the bending occurs during thunniform locomotion. *C*, Tendons are very long relative to fibers, suggesting that they may stretch and affect fiber dynamics.

individual tendon was on average 21 times higher than its own toughness at the inflection point.

The anatomical dissection and tensile testing revealed that the tendons are likely preloaded and that the properties of the tendons vary along the length of the fish. During dissection, the individual tendons recoiled when cut even though the spine of the tuna was neutral. Removal of all tendons from one side of the fish resulted in spinal curvature away from the cut side. Thus, we cannot predict what range of the highly nonlinear tendon stress-strain curve is used in vivo. The tensile testing showed moderate trends in the elongation parameters with anterior-posterior position, while the stress parameters did not vary: posterior tendons had 2.2% more elongation than anterior tendons at onset of plastic deformation and failed at 6.4% greater elongation than anterior tendons.

Discussion

Tunas possess a unique combination of musculoskeletal and physiological characteristics (reviewed in Graham and Dickson

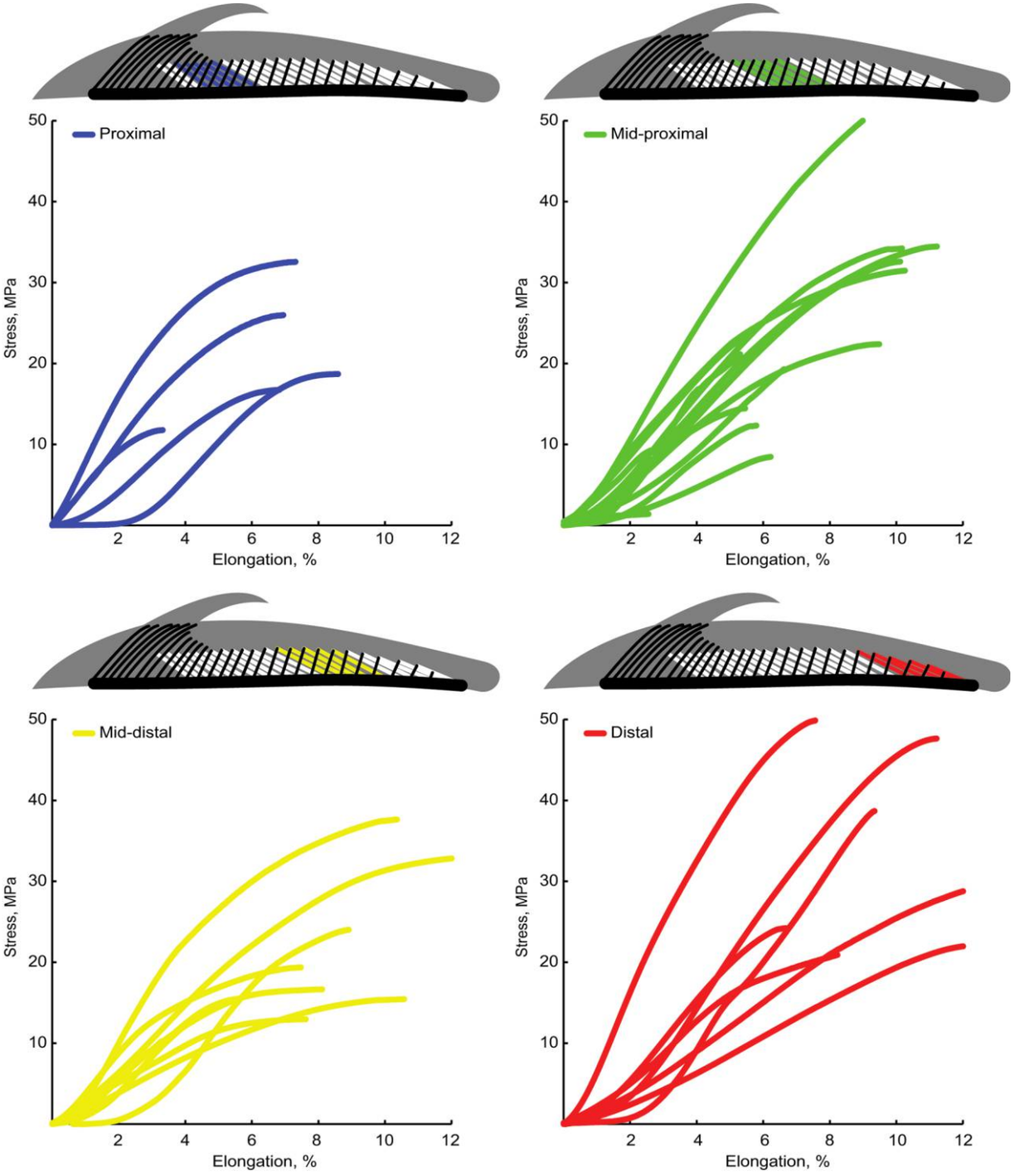

Figure 7. Tendon tensile properties. Most traces show the typical toe region, minimal linear ranges, and ductile failure modes (decreasing stiffness at failure). Tendons were from an 82-cm Pacific bluefin.

2001; Korsmeyer and Dewar 2001; Westneat and Wainwright 2001) that powers their long-distance cruising across oceans (Block et al. 2001). The tuna's slow-twitch red muscle that powers these migrations is compactly arranged as part of the muscle cone morphology (Fierstine and Walters 1968; Westneat and Wainwright 2001), allowing a high physiological cross-sectional area within a fusiform body shape (Westneat and Wainwright 2001; Katz 2002). The red muscle is connected to the spine and tail through long tendons (Fierstine and Walters 1968; Westneat et al. 1993). In terrestrial animals, long tendons are known to greatly improve running economy by stretching to allow muscle fibers to operate near optimal lengths and velocities and by storing

Table 1: Tendon mechanical properties

Tendon property	At inflection	At failure
Elongation (%)	2.9 ± 1.4	8.7 ± 3.1
Force (N)	21.3 ± 10.8	33 ± 21
Stress (MPa)	13.6 ± 6.8	25.5 ± 11.6
Elastic modulus (MPa/(m/m))	501 ± 187	0[a]
Toughness (kJ/m^3)	107 ± 89	1,326 ± 951

[a]For the ductile failure mode, failure point was defined as the point at which the elastic modulus was 0.

elastic energy (Biewener and Roberts 2000). Here, we studied the force-generating capacity of tuna red muscle and the stiffness and breaking strength of POTs to determine whether these tendons could also play a role in the swimming economy of the tuna.

The tensile testing of the tuna tendons, combined with our estimates of the strength of the myomeres, indicates that the POTs likely do stretch during locomotion but that the POTs are not the main force transmission pathway between the red muscle and the spine. There are two alternate pathways for red muscle force: (1) through the red muscle myomeres to the tail via the GLT and (2) via the AOTs to the skin (e.g., Westneat et al. 1993). It is possible that a large fraction of the myomere force is transmitted to the posteriorly adjacent myomere, while a smaller fraction of the load is transmitted to the POT. As in the other scombrids investigated by Westneat et al. (1993), the most posterior red muscle segments of myomeres are connected from their anterior myomere neighbors to the GLT; they do not have associated POTs. This structure provides a potential pathway by which the forces of the red muscle farther anterior in the body can be transmitted to the tail instead of to the spine via the POTs. This load transmission pathway is consistent with two observations of the red muscle activation pattern observed in yellowfin (Knower et al. 1999). First, the anterior red muscle myomeres activate at the beginning of the tail-beat cycle and remain activated as the wave of activation progresses posteriorly, and finally, they deactivate nearly synchronously. Second, the GLT loading starts synchronously with the activation of the anterior myomeres (reviewed in Katz 2002). In pathway 2, the myomeres could transmit force laterally through the AOTs to the skin, as suggested by Westneat et al. (1993). In our specimens, the AOTs appeared as distributed collagen mesh and could not have been mechanically isolated or tested.

The questions of whether and how tendons affect tuna swimming economy have previously been investigated in a smaller (2 kg) yellowfin (Knower et al. 1993). The authors suggested that energy storage in the GLT was not significant (Knower et al. 1993), based on <1% tendon strain observed in vivo with a buckle transducer on the GLT. However, with long tendons and short muscle fibers, it is possible that a small percent strain in a long tendon can still affect muscle fiber contractile dynamics by a large fraction of the fiber length and thus impact swimming economy. Interestingly, Syme and Shadwick (2002) calculate that the red muscle is capable of generating much larger loads than the 4 N that was measured by Knower et al. (1993) in the GLT in vivo and thus speculate that the POTs or other load transmission pathways may be important. The stiffer GLT may serve to transfer load through a narrow anatomy with high precision, such as the long tendons in the human wrist (Loren and Lieber 1995). There is not enough information available to reconcile the forces to examine this theory. It is also unknown how the measurements of GLT strain in vivo would scale with body mass. Our measurements of the lengths and relative positions of the spine, epicentral bone, and tendon could aid in creating models to test these hypotheses. It is possible that elastic energy storage or tuning of muscle fiber dynamics is accomplished by a combination of the myomeres in series and the POTs.

Our observations of the systematic variation in muscle aspect ratio and differences between fish of different sizes are the first quantification of red muscle PCSA and distribution within the muscle cones. It is widely accepted that cone morphology of fish muscles enables packing of large PCSA of muscle into a body volume (Westneat et al. 1993; Westneat and Wainwright 2001). If all the myomere force was transmitted in series to the adjacent myomere, we would predict the same PCSA in each myomere, as observed in the smaller specimen in our study. The observation in the larger fish that the PCSA of the more posterior myomeres is larger than that of the anterior myomeres suggests that the muscle loading in these fish is not only through the series of myomeres but also through other load transmission pathways. This observation suggests that the load transmission pathways may play differential roles across stages of growth. Other changes in red muscle with growth are the decrease in fast-twitch oxidative-glycolytic fibers within the red muscle (Roy et al. 2012) and the decrease in the proportion of red muscle mass relative to body weight (Graham et al. 1983).

Our conclusions that the POTs cannot be the primary load pathway for the red muscle depends on Syme and Shadwick's (2002) estimate that the red muscle in yellowfin tuna can generate 14.0 N/cm^2: if the red muscle can generate these stresses, the PCSA of the myomeres we measured in a similar-sized fish (19.5 ± 2.3 cm^2) would mean that each myomere could easily break its associated tendon (33 ± 21 N). Additionally, the hypaxial red muscle also loads the same tendons. We suspect that Syme and Shadwick's estimate for the peak stress of red muscle is reasonable given that similar peak stresses have been measured in rainbow trout and largemouth bass (Coughlin 2000) and in scup (Rome and Swank 1992). Since the measurements of Coughlin (2000) and Rome et al. (1992) were made by electrically stimulating muscle fibers in vitro, it is possible that

the muscle stresses experienced in vivo are lower. It is possible that the large cross-sectional area of the red muscle tissue is not used to produce large forces but instead used to provide a large pool of fresh fibers, so that as motor units fatigue, activation can be increased and additional motor units recruited (e.g., Lieber 2010). Evidence of orderly recruitment in fish has been observed using electromyography in skipjack tuna (Brill and Dizon 1979) and in carp (Rome et al. 1984), in that red muscle is recruited at low speeds and white muscle is additionally recruited at higher speeds. The hypothesis of orderly recruitment within red muscle of tuna is supported by histological observations of a range of fiber sizes and differential levels of metabolic activity between red muscle fibers of Pacific bluefin tuna (Roy et al. 2012). Our result also depends on comparing tendon measurements and PCSA measurements from two different fish of similar lengths: 79 cm (PCSA) and 82 cm (tendons).

Compared with existing data for tuna great lateral tendons, the tendons we tested from Pacific bluefin tuna were not as stiff but failed at similar stresses and with similar modes of failure. On average, the maximum tangential stiffness of the POTs we tested was 501 ± 187 MPa, which is lower than previous measurements of the GLTs in the tails of yellowfin (1.43 ± 0.29 GPa) and albacore tuna (1.19 ± 0.15 GPa; Shadwick et al. 2002) and is also lower than mammalian tendons across multiple species (approximately 1.5 GPa; Bennett et al. 1986; Pollock and Shadwick 1994). Tendons may increase in cross-sectional area and stiffness in response to loading (reviewed in Heinemeier and Kjaer 2011). It is possible that the greater stiffness of the GLTs relative to the POTs could be a tissue response to differential loading if the GLTs are loaded more than the POTs during swimming. The differences we observed might be due to differences in the species and size of the tuna examined: we tested the POTs from an 82-cm Pacific bluefin tuna (11.8 kg), whereas Shadwick et al. (2002) made measurements on juveniles (1–2 kg yellowfin and 4–5 kg albacore). The breaking stress of the POTs we measured was 25.5 ± 11.6 MPa, which is similar to the breaking stress in the GLTs (30 MPa; Shadwick et al. 2002) but much lower than the breaking stress in mammalian tendons (80–120 MPa; Bennett et al. 1986). Furthermore, the failure mode in both the tendons we tested and those of Shadwick et al. (2002) was a gradual ductile failure, which contrasts with the abrupt rupturing failure mode that is characteristic of mammalian tendons (Bennett et al. 1986; Shadwick 1990).

Like many terrestrial animals, tunas have very long tendons that are attached to strong muscles with large cross-sectional areas. Although we believe it is clear from our work that these tendons are stretched during swimming, the load that these tendons can bear constitutes a fraction of the forces the red muscle is capable of generating. Thus, further study of the anatomy of alternate load transmission pathways is critical for a complete biomechanical understanding of red-muscle-powered thunniform swimming. Future work measuring and modeling the load-bearing pathways of tuna anatomy and forces on the tail and spine during swimming would enable estimates of the tendon-fiber dynamics powering these sophisticated swimmers. Advances in accelerometry measurement in free-swimming fish (Tsuda et al. 2006; Gleiss et al. 2011, 2019), three-dimensional models of skeletal muscle (Blemker and Delp 2005), and computational models of muscle-tendon dynamics (e.g., Delp et al. 2007; Millard et al. 2013; Seth et al. 2018) could enable such future studies. Simulation can also help examine comparative advantages of convergent evolution—for example, lamnid sharks also convergently evolved internally located, warm red muscle (Carey et al. 1985) but without a tendon structure like the scombrids (Donley et al. 2004) and with a different locomotory style, subcarangiform swimming (e.g., Gemballa et al. 2006).

Acknowledgments

Collection of tunas was supported by Stanford University and the Monterey Bay Aquarium Foundation. We thank Alex Norton and Ethan Estess for live tuna specimen care and handling at the Tuna Research and Conservation Center. We thank Robert Schallert for specimen collection. We thank the Woods Hole Oceanographic Institution scientists and Dr. Darlene Ketten of Woods Hole Oceanographic Institution for enabling the computed tomogaphy scan.

Literature Cited

Altringham J.D. and B.A. Block. 1997. Why do tuna maintain elevated slow muscle temperatures? power output of muscle isolated from endothermic and ectothermic fish. J Exp Biol 200:2617–2627.

Altringham J.D. and R.E. Shadwick. 2001. Swimming and mus cle function. Pp. 314–341 in B.A. Block and E.D. Stevens, eds. Fish physiology. Vol. 19. Tuna: physiology, ecology, and evolution. Academic Press, San Diego, CA.

Arnold E.M. and S.L. Delp. 2011. Fibre operating lengths of human lower limb muscles during walking. Philos Trans R Soc B 366:1530–1539.

Arnold E.M., S.R. Ward, R.L. Lieber, and S.L. Delp. 2010. A model of the lower limb for analysis of human movement. Ann Biomed Eng 38:269–279.

Bennett M.B., R.F. Ker, N.J. Dimery, and R.M. Alexander. 1986. Mechanical properties of various mammalian tendons. J Zool (Lond) A 209:537–548.

Bernal D., K.A. Dickson, R.E. Shadwick, and J.B. Graham. 2001. Analysis of the evolutionary convergence for high performance swimming in lamnid sharks and tunas. Comp Biochem Physiol 129:695–726.

Bernal D., J.M. Donley, D.G. McGillivray, S.A. Aalbers, D.A. Syme, and C. Sepulveda. 2010. Function of the medial red muscle during sustained swimming in common thresher sharks: contrast and convergence with thunniform swimmers. Comp Biochem Physiol A 155:454–463.

Biewener A.A., D.D. Konieczynski, and R.V. Baudinette. 1998. In vivo muscle force-length behavior during steady-speed hopping in tammar wallabies. J Exp Biol 201:1681–1694.

Biewener A.A. and T.J. Roberts. 2000. Muscle and tendon contributions to force, work, and elastic energy savings: a comparative perspective. Exerc Sport Sci Rev 28:99–107.

Blemker S. and S. Delp. 2005. Three-dimensional representation of complex muscle architectures and geometries. Ann Biomed Eng 33:661–673.

Block B.A., H. Dewar, S.B. Blackwell, T.D. Williams, E.D. Prince, C.J. Farwell, A. Boustany, et al. 2001. Migratory movements, depth preferences, and thermal biology of Atlantic bluefin tuna. Science 293:1310–1314.

Block B.A., J.R. Finnerty, A.F.R. Stewart, and J. Kidd. 1993. Evolution of endothermy in fish: mapping evolution of endothermy physiological traits on a molecular phylogeny. Science 260:210–214.

Brill R.W. and A.E. Dizon. 1979. Red and white muscle fibre activity in swimming skipjack tuna, *Katsuwonus pelamis* (L.). J Fish Biol 15:679–685.

Carey F.G., J.G. Casey, H.L. Pratt, D. Urquhart, and J.E. McCosker. 1985. Temperature, heat production and heat exchange in lamnid sharks. Mem S Calif Acad Sci 9:92–108.

Carey F.G. and K.D. Lawson. 1973. Temperature regulation in free-swimming bluefin tuna. Comp Biochem Physiol A 44: 375–392.

Carey F.G. and J.M. Teal. 1966. Heat conservation in tuna fish muscle. Proc Natl Acad Sci USA 56:1464–1469.

Cipolla K.M. 2014. Characterization of the boundary layers on full-scale bluefin tuna. NUWC-NPT Technical Report 12,163. Naval Undersea Warfare Center Division, Newport, RI.

Coughlin D.J. 2000. Power production during steady swimming in largemouth bass and rainbow trout. J Exp Biol 203: 617–629.

Delp S.L., F.C. Anderson, A.S. Arnold, P. Loan, A. Habib, C.T. John, E. Guendelman, and D.G. Thelan. 2007. OpenSim: open-source software to create and analyze dynamic simulations of movement. IEEE Trans Biomed Eng 55:1940–1950.

Dewar H. and J. Graham. 1994. Studies of tropical tuna swimming performance in a large water tunnel—kinematics. J Exp Biol 192:45–59.

Dickson K.A and J.B. Graham. 2004. Evolution and consequences of endothermy in fishes. Physiol Biochem Zool 77: 998–1018.

Donley J.M., C.A. Sepulveda, P. Konstantinidis, S. Gemballa, and R.E. Shadwick. 2004. Convergent evolution in mechanical design of lamnid sharks and tunas. Nature 429:61–65.

Donley J.M., R.E. Shadwick, C.A. Sepulveda, P. Konstantinidis, and S. Gemballa. 2005. Patterns of red muscle strain/activation and body kinematics during steady swimming in a lamnid shark, the shortfin mako (*Isurus oxyrinchus*). J Exp Biol 208:2377–2387.

Ellerby D.J., J.D. Altringham, T. Williams, and B.A. Block. 2000. Slow muscle function of pacific bonito (*Sarda chiliensis*) during steady swimming. J Exp Biol 203:2001–2013.

Fierstine H.L. and V. Walters. 1968. Studies in locomotion and anatomy of scombroid fishes. Southern California Academy of Sciences, Los Angeles.

Gemballa S., K. Hagen, K. Roder, M. Rolf, and K. Treiber. 2003. Structure and evolution of the horizontal septum in vertebrates. J Evol Biol 16:966–975.

Gemballa S., P.D. Konstantinidis, J.M. Donley, C. Sepúlveda, and R.E. Shadwick. 2006. Evolution of high-performance swimming in sharks: transformations of the musculotendinous system from subcarangiform to thunniform swimmers. J Morphol 267:477–493.

Gleiss A.C., R.J. Schallert, J.J. Dale, S.G. Wilson, and B.A. Block. 2019. Direct measurement of swimming and diving kinematics of giant Atlantic bluefin tuna (*Thunnus thynnus*). R Soc Open Sci 6:190203.

Gleiss A.C., R.P. Wilson, and E.L.C. Shepard. 2011. Making overall dynamic body acceleration work: on the theory of acceleration as a proxy for energy expenditure. Methods Ecol Evol 2:23–33.

Graham J.B. and K.A. Dickson. 2000. The evolution of thunniform locomotion and heat conservation in scombrid fishes: new insights based on the morphology of *Allothunnus fallai*. Zool J Linn Soc 129:419–466.

———. 2001. Anatomical and physiological specializations for endothermy. Pp. 121–166 in B.A. Block and E.D. Stevens, eds. Tuna: physiology, ecology, and evolution. Academic Press, San Diego, CA.

Graham J.B., F.J. Koehrn, and K.A. Dickson. 1983. Distribution and relative proportions of red muscle in scombrid fishes: consequences of body size and relationships to locomotion and endothermy. Can J Zool 61:2087–2096.

Heinemeier K.M. and M. Kjaer. 2011. In vivo investigation of tendon responses to mechanical loading. J Musculoskelet Neuronal Interact 11:115–123.

Huang C-Y., V.M. Wang, E.L. Flatow, and V.C. Mow. 2009. Temperature-dependent viscoelastic properties of the human supraspinatus tendon. J Biomech 42:546–549.

Huang H., J. Zhang, K. Sun, X. Zhang, and S. Tian. 2011. Effects of repetitive multiple freeze-thaw cycles on the biomechanical properties of human flexor digitorum superficialis and flexor pollicis longus tendons. Clin Biomech 26:419–423.

Jung H.-J., G. Vangipuram, M.B. Fisher, G. Yang, S. Hsu, J. Bianchi, C. Ronholdt, and S.L.-Y. Woo. 2011. The effects of multiple freeze-thaw cycles on the biomechanical properties of the human bone-patellar tendon-bone allograft. J Orthop Res 29:1193–1198.

Katz S.L. 2002. Review: design of heterothermic muscle in fish. 205:2251–2266.

Katz S.L., D.A. Syme, and R.E. Shadwick. 2001. Enhanced power in yellowfin tuna. Nature 410:770–771.

Kishinouye K. 1923. Contributions to the comparative study of the so-called scombroid fishes. J Coll Agric Imp Univ Tokyo 8:293–475.

Knower T., R.E. Shadwick, A.A. Biewener, K.E. Korsmeyer, and J.B. Graham. 1993. Direct measurement of tail tendon forces in swimming tuna. Am Zool 33:30A.

Knower T., R.E. Shadwick, S.L. Katz, J.B. Graham, and C.S. Wardle. 1999. Red muscle activation patterns in yellowfin (*Thunnus albacares*) and skipjack (*Katsuwonus pelamis*) tuna during steady swimming. J Exp Biol 202:2127–2138.

Korsmeyer K.E. and H. Dewar. 2001. Tuna metabolism and energetics. Pp. 36–71 in B.A. Block and E.D. Stevens, eds.

Tuna: physiology, ecology, and evolution. Academic Press, San Diego, CA.

Lieber R.L. 2010. Skeletal muscle physiology. Pp. 41–92 in Skeletal muscle structure, function, and plasticity. Lippincott Williams Wilkins, Baltimore.

Loren G.J. and R.L. Lieber. 1995. Tendon biomechanical properties enhance human wrist muscle specialization. J Biomech 28:791–799.

Millard M., T. Uchida, A. Seth, and S.L. Delp. 2013. Flexing computational muscle: modeling and simulation of musculotendon dynamics. J Biomech Eng 135:21005.

Moon D.K., S.L.-Y. Woo, Y. Takakura, M.T. Gabriel, and S.D. Abramowitch. 2006. The effects of refreezing on the viscoelastic and tensile properties of ligaments. J Biomech 39:1153–1157.

Pollock C.M. and R.E. Shadwick. 1994. Allometry of muscle, tendon, and elastic energy storage capacity in mammals. Am J Physiol 266:R1022–R1031.

Rome L.C., I. Choi, G. Lutz, and A. Sosnicki. 1992. The influence of temperature on muscle function in the fast swimming scup. I. Shortening velocity and muscle recruitment during swimming. J Exp Biol 163:259–279.

Rome L.C., P.T. Loughna, and G. Goldspink. 1984. Muscle fiber activity in carp as a function of swimming speed and muscle temperature. Am J Physiol 247:R272–279.

Rome L.C. and D. Swank. 1992. The influence of temperature on power output of scup red muscle during cyclical length changes. J Exp Biol 171:261–281.

Roy B.C., M. Ando, M. Nakatani, T. Okada, Y. Sawada, T. Itoh, and Y. Tsukamasa. 2012. Muscle fiber types, growth and development in the whole myotome of cultured Pacific bluefin tuna *Thunnus orientalis*. Fish Sci 78:471–483.

Rueden C.T., J. Schindelin, M.C. Hiner, B.E. DeZonia, A.E. Walter, E.T. Arena, and K.W. Eliceiri. 2017. ImageJ2: imageJ for the next generation of scientific image data. BMC Bioinform 18:529.

Schindelin J., I. Arganda-Carreras, E. Frise, V. Kaynig, M. Longair, T. Pietzsch, S. Preibisch, et al. 2012. Fiji: an open-source platform for biological-image analysis. Nat Methods 9:676–682.

Seth A., J.L. Hicks, T.K. Uchida, A. Habib, C.L. Dembia, J.J. Dunne, C.F. Ong, et al. 2018. OpenSim: simulating musculoskeletal dynamics and neuromuscular control to study human and animal movement. PLoS Comp Biol 14:e1006223.

Shadwick R.E. 1990. Elastic energy storage in tendons: mechanical differences related to function and age. J Appl Physiol 68:1033–1040.

Shadwick R.E. and S. Gemballa. 2006. Structure, kinematics, and muscle dynamics in undulatory swimming. Pp. 241–280 + fig. 7.15 in R.E. Shadwick and G.V. Lauder, eds. Fish biomechanics. Academic Press, San Diego, CA.

Shadwick R.E., H.S. Rapoport, and J.M. Fenger. 2002. Structure and function of tuna tail tendons. Comp Biochem Physiol A 133:1109–1125.

Shadwick R.E. and D.A. Syme. 2008. Thunniform swimming: muscle dynamics and mechanical power production of aerobic fibres in yellowfin tuna (*Thunnus albacares*). J Exp Biol 211:1603–1611.

Sharkey N.A., T.S. Smith, and D.C. Lundmark. 1995. Freeze clamping musculo-tendinous junctions for in vitro simulation of joint mechanics. J Biomech 28:631–635.

Syme D.A. and R.E. Shadwick. 2002. Effects of longitudinal body position and swimming speed on mechanical power of deep red muscle from skipjack tuna (*Katsuwonus pelamis*). J Exp Biol 205:189–200.

———. 2011. Red muscle function in stiff-bodied swimmers: there and almost back again. Philos Trans R Soc B 366: 1507–1515.

Triantafyllou M.S., F.S. Hover, A.H. Techet, and D.K.P. Yue. 2005. Review of hydrodynamic scaling laws in aquatic locomotion and fishlike swimming. Appl Mech Rev 58:226–237.

Tsuda Y., R. Kawabe, H. Tanaka, Y. Mitsunaga, T. Hiraishi, K. Yamamoto, and K. Nashimoto. 2006. Monitoring the spawning behaviour of chum salmon with an acceleration data logger. Ecol Freshw Fish 15:264–274.

Videler J.J. 1993. Fish swimming. Chapman and Hall, London.

Westneat M.W., W. Hoese, C.A. Pell, and S.A. Wainwright. 1993. The horizontal septum: mechanisms of force transfer in locomotion of scombrid fishes (Scombridae, Perciformes). J Morphol 204:183–204.

Westneat M.W. and S.A. Wainwright. 2001. Mechanical design for swimming: muscle, tendon, and bone. Pp. 271–311 in B.A. Block and E.D. Stevens, eds. Tuna: physiology, ecology, and evolution. Academic Press, San Diego, CA.